ACS APPLIED MATERIALS & INTERFACES

Letter

www.acsami.org

Sn−Cu Nanocomposite Anodes for Rechargeable Sodium-Ion Batteries

Yong-Mao Lin,[†] Paul R. Abel,[†] Asha Gupta,[‡,§] John B. Goodenough,[‡,§,⊥,∥] Adam Heller,[†,⊥] and C. Buddie Mullins*[,†,‡,⊥,∥,#]

[†]McKetta Department of Chemical Engineering, [#]Department of Chemistry and Biochemistry, [⊥]Center for Electrochemistry, [‡]Texas Materials Institute, [§]Materials Science and Engineering Program, and [∥]Center for Nano- and Molecular Science, University of Texas at Austin, 1 University Station, C0400 Austin, Texas 78712-0231, United States

Supporting Information

ABSTRACT: $Sn_{0.9}Cu_{0.1}$ nanoparticles were synthesized via a surfactant-assisted wet chemistry method, which were then investigated as an anode material for ambient temperature rechargeable sodium ion batteries. The $Sn_{0.9}Cu_{0.1}$ nanoparticle-based electrodes exhibited a stable capacity of greater than 420 mA h g^{-1} at 0.2 C rate, retaining 97% of their maximum observed capacity after 100 cycles of sodium insertion/deinsertion. Their performance is considerably superior to electrodes made with either Sn nanoparticles or Sn microparticles.

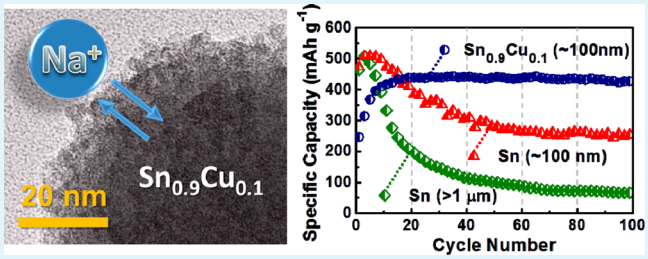

KEYWORDS: *tin copper alloy, nanoparticles, anode, Na-ion battery*

INTRODUCTION

Electrical energy storage is of growing importance for both stationary and mobile applications. Among energy storage systems, rechargeable lithium-based batteries have been studied because lithium has the most negative reduction potential (−3.04 V vs standard hydrogen electrode, SHE) and the lowest density (0.53 g cm^{-3}) of all metals.[1] Currently, Li-ion batteries are widely adopted to power portable electronic devices. However, their high price remains a daunting challenge in medium to large-scale energy storage required for transportation or grid energy storage.[2−4] Lithium is a relatively rare element among light metals, its concentration in the upper continental crust is estimated to be 35 ppm.[5] Sodium, unlike lithium, is much more abundant on earth, where the sodium concentration is estimated to be 10 320 ppm in seawater and 28 300 ppm in the lithosphere.[6] Consequently, in those applications where the amount of electrode material is large enough to substantially affect the cost, the use of sodium is advantageous. The low reduction potential of Na (−2.71 V vs SHE) also makes it an attractive material for energy storage. Molten-salt batteries containing sodium, e.g., Na/S and Na/$NiCl_2$ batteries,[7,8] have been developed as inexpensive energy storage systems when compared to lithium-ion batteries. However, these molten-salt batteries need to operate at high temperatures (250 to 350 °C) to keep the electrodes in liquid form, which makes it more difficult for designing battery systems that meet stringent safety requirements. Therefore, it is important to develop an affordable secondary Na-ion battery that can be cycled at ambient temperature.

Current commercial Li-ion batteries are comprised of lithium metal oxide as the cathode material and graphite as the lithium host anode material. The electrical energy is stored via the difference of chemical potential of lithium between the cathode and the anode. A similar mechanism can be applied to Na-ion batteries. Most of the recent studies of Na-ion batteries have been focused on cathode materials.[9,10] However, graphite cannot be readily used as the anode material for Na-ion batteries, because for sodium atoms it is more kinetically favorable to electroplate onto the surface of graphite than to intercalate into its basal planes. Stevens and Dahn showed that only a trace amount of sodium can intercalate into graphite (~NaC_{186}).[11] Thus far, few materials have been considered for Na-ion anodes. Sb has been reported as a candidate anode material for Na storage, exhibiting a high reversible capacity of ~600 mA g^{-1}.[12,13] Additionally, Chevrier and Ceder predicted from density functional theory calculations that Na alloys of Si, Ge, Sn, and Pb, could also be used as anode materials for Na-ion batteries.[14] Among these materials, tin is of great interest because of its high theoretical capacity 847 mA h g^{-1} or 6164 mA h cm^{-3}, corresponding to the most sodium-rich phase $Na_{15}Sn_4$.[14−16] Nohira and Hagiwara et al. found an initial reversible capacity as high as 729 mAh g^{-1} for sodium storage using a Sn thin film electrode.[17] However, the capacity was not well retained, decreasing to 121 mA h g^{-1} as early as the 10th cycle. Additionally, Ellis, Ferguson, and Obrovac observed a first cycle capacity of above 800 mA h/g in a slurry-cast Sn electrode; however, the capacity decayed to zero within five cycles.[18] The rapid degradation of the Sn electrode, in both

Received: June 20, 2013
Accepted: August 19, 2013
Published: August 19, 2013

   dx.doi.org/10.1021/am4023994 | ACS Appl. Mater. Interfaces 2013, 5, 8273−8277

cases, was attributed to the volume change during sodium insertion/deinsertion. Because nanostructured materials can superplastically deform, they can sustain very large strains, of more than 200% elongation.[19,20] However, Sn nanoparticles are thermodynamically unstable relative to Sn microparticles that tend to aggregate to reduce their large surface energy.[21,22] Intermetallic alloy anodes show better electrochemical performance for lithium-ion insertion/deinsertion because of lesser aggregation of their electroactive particles.[23] In Na-ion batteries, Sn nanocomposite anodes, such as Sn/C[24] and SnSb/C,[25] exhibited improved cycling stability, but their capacities still dropped noticeably after fewer than 50 cycles. Therefore, a core challenge to address in safer sodium alloy anodes is that of cycling stability upon the alloying/dealloying of sodium.

Sn/Cu nanocomposites have been studied as anode materials for lithium-ion batteries, with the addition of copper to the nanostructures significantly improving the stability of the material.[26−28] Additionally, phase-pure η-Cu6Sn5 has been studied as an anode material for sodium-ion batteries.[29] The diffusion depth of Na in η-Cu6Sn5 was found to be limited to ~3 nm because of the large size of the sodium ion.

Here we report on $Sn_{0.9}Cu_{0.1}$ nanoparticles that provide promising Na-ion battery anodes. The nanoparticles were prepared at room temperature through a surfactant-assisted wet chemistry route, where aqueous Sn^{2+} and Cu^{2+} ions in a molar ratio of 9:1 were reduced by using sodium borohydride ($NaBH_4$) in the presence of the surfactant 1,2-diaminopropane. Details of the preparation procedure are provided in the Supporting Information. The electrochemical characteristics of the prepared $Sn_{0.9}Cu_{0.1}$ nanoparticles were compared to those of commercially available Sn nanoparticles and Sn microparticles.

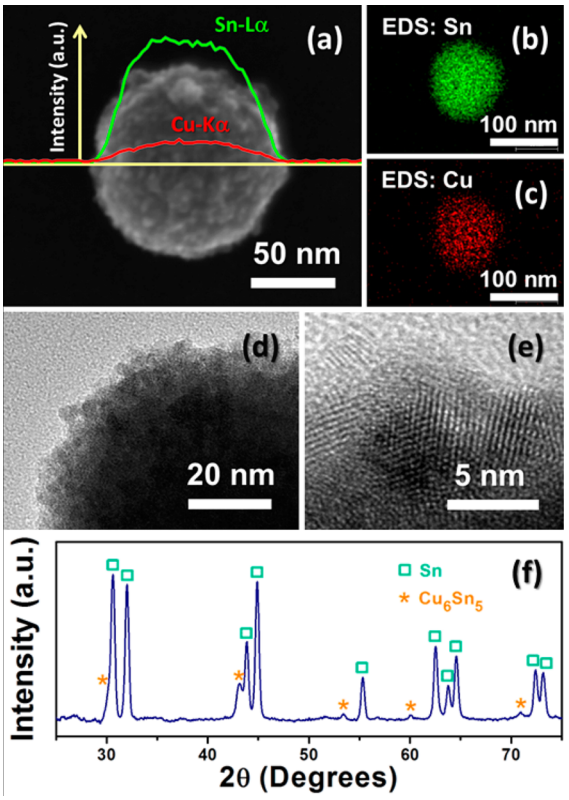

Figure 1. (a) SEM image of a single $Sn_{0.9}Cu_{0.1}$ particle with EDS line scan across the particle; EDS mapping for element (b) Sn and (c) Cu; TEM images of a single $Sn_{0.9}Cu_{0.1}$ particle examined under (d) low magnification and (e) high magnification; (f) X-ray diffraction pattern of the $Sn_{0.9}Cu_{0.1}$ powder.

RESULTS AND DISCUSSION

A scanning electron microscope (SEM) image shows that the average diameter of the $Sn_{0.9}Cu_{0.1}$ particles is 100 ± 34 nm with the error given as one standard deviation (see Figure S1a in the Supporting Information). Energy-dispersive X-ray spectroscopy (EDS) of the nanocomposite showed (see Table S1 in the Supporting Information) an average Sn/Cu molar ratio of 0.896/0.104. A SEM image of a typical Sn/Cu particle taken at a higher magnification is shown in Figure 1a, with a linear EDS scan performed across the center of the particle. The EDS line-scan shows that the composition of the particle is spatially homogeneous. EDS elemental mapping confirmed that Sn and Cu are uniformly distributed in the nanocomposite (Figure 1b, c). Transmission electron microscopy (TEM) shows that the $Sn_{0.9}Cu_{0.1}$ nanocomposite particle is actually composed of multiple small monocrystals (Figure 1d), each much smaller than the particle (Figure 1e). The powder X-ray diffraction (XRD) pattern of the as-prepared $Sn_{0.9}Cu_{0.1}$ nanoparticles shows a tin-rich composite made of crystalline Sn and Cu_6Sn_5 (Figure 1f). The full width at half-maximum (fwhm) for the XRD features is ~0.5°. Application of the Scherrer equation gives a minimum crystallite size of ~16 nm, which is consistent with the polycrystalline nature of the particles.

The electrochemical performance of the prepared $Sn_{0.9}Cu_{0.1}$ nanoparticles was evaluated in 2032 type coin cells. Commercially available Sn nanoparticles with an average diameter of 125 ± 38 nm (error given as one standard deviation) and Sn microparticles (>1 μm), with their SEM images shown in Figure S1b, c and their XRD patterns shown in Figure S2 in the Supporting Information, were employed as references for comparison with the $Sn_{0.9}Cu_{0.1}$ nanoparticles. The electrodes were prepared by slurry casting of 80% of either $Sn_{0.9}Cu_{0.1}$ or the reference Sn, 10% sodium carboxymethyl cellulose (Na-CMC) binder, and 10% carbon black as the conductive additive. Cells were assembled and tested against a sodium−metal foil counter/reference electrode with 1 M $NaPF_6$ in fluoroethylene carbonate (FEC)/diethyl carbonate (DEC) (1/1 wt/wt) as the electrolyte. FEC as an additive or as a cosolvent in the electrolyte has been shown to improve the electrochemical performance of both Li-ion and Na-ion batteries.[12,13,30−34]

The assembled cells were cycled between 10 mV and 750 mV vs Na/Na^+ at a 0.2 *C* rate (169 mA per gram of Sn), corresponding to a rate of fully charging or discharging the cell within 5 h. The upper cutoff voltage was limited to 750 mV to improve the cyclability.[35] The discharge capacities for one hundred cycles for electrodes made with the $Sn_{0.9}Cu_{0.1}$ nanocomposite, Sn nanoparticles, and Sn microparticles are shown in Figure 2a. The changes in the capacities of the electrodes made with Sn nanoparticles and Sn microparticles were similar in the first few cycles, both reaching their maximum capacity of ~510 mA h g^{-1} after 3 cycles. Capacity being independent of size implies rapid diffusion of sodium in Sn. However, the capacity is much lower than theoretical, which implies slow diffusion of sodium in Sn. This is consistent with the results of Xu et al., who reported that the diffusion of sodium in Sn was much slower than the diffusion of lithium in Sn.[24] The similar capacities of the Sn microparticles and

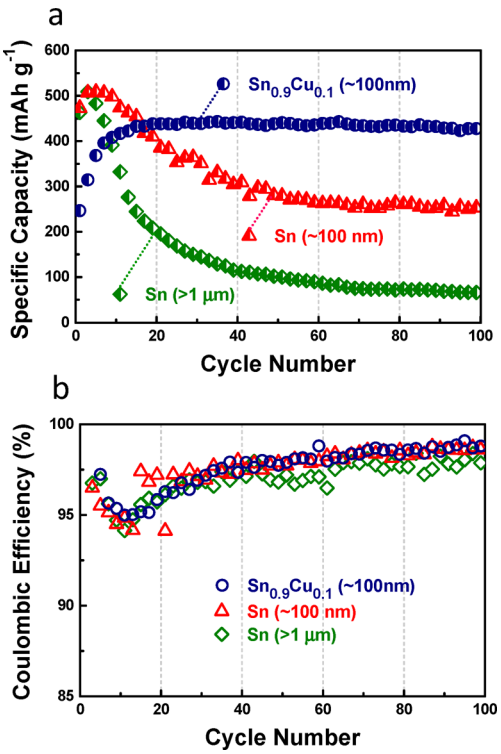

Figure 2. (a) Reversible discharge capacities and (b) Coulombic efficiencies of electrodes made of $Sn_{0.9}Cu_{0.1}$ nanoparticles, Sn nanoparticles, and Sn microparticles. All electrodes cycled at 0.2 *C* rate (169 mA g^{-1}).

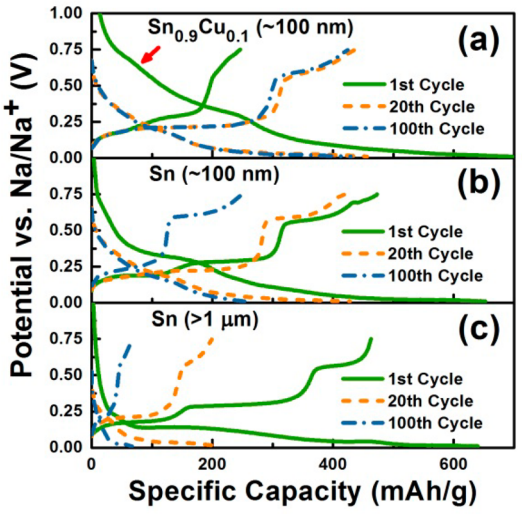

Figure 3. Voltage profiles of electrodes made of (a) $Sn_{0.9}Cu_{0.1}$ nanoparticles, (b) Sn nanoparticle,s and (c) Sn microparticles. All electrodes cycled at 0.2 *C* rate (169 mA g^{-1}). The red arrow indicates an additional feature for the $Sn_{0.9}Cu_{0.1}$ electrode in the initial Na insertion process.

nanoparticles could be due to cracking of the microparticles during sodiation. The cracks would allow sodiation of the particles interior.

The capacity of the electrode made of larger Sn particles (>1 μm) dropped much more rapidly than that made of smaller particles (~100 nm), showing that the large volume change upon cycling is better accommodated by small particles. After 100 cycles, the capacities of the electrodes made of Sn nanoparticles and Sn microparticles decreased respectively to 250 and 66 mA h g^{-1}, i.e., only 49% and 13% of their maximum capacity was retained, suggestive of volume-change associated electrochemical agglomeration of the Sn nanoparticles, similar to that observed in Li/Sn alloys.[21−23]

The reversible capacity of the $Sn_{0.9}Cu_{0.1}$ electrode was 250 mA h g^{-1} in the initial cycle, gradually increasing to ~440 mA h g^{-1} (just over half of theoretical) after 20 cycles (Figure 2a). A slow increase in capacity has been observed previously and is not well understood.[32,36−38] The added mass of copper accounts for the lesser specific maximum capacity of $Sn_{0.9}Cu_{0.1}$ versus that of Sn, because Cu does not form an alloy with sodium. However, compared to the Sn-based electrodes, the $Sn_{0.9}Cu_{0.1}$ nanoparticle electrode shows significantly improved stability during prolonged sodium insertion/deinsertion cycling, with 97% of the reversible capacity being retained between the 20th cycle and the 100th cycle. The Coulombic efficiencies for electrodes made with the $Sn_{0.9}Cu_{0.1}$ nanocomposite, Sn nanoparticles and Sn microparticles are shown in Figure 2b. Despite the differences in stability between the materials, the Coulombic efficiencies are very similar.

Figure 3 shows the voltage profiles of electrodes made of $Sn_{0.9}Cu_{0.1}$ nanoparticles, Sn nanoparticles and Sn microparticles for cycles 1, 20, and 100 at 0.2 *C* rate. In the initial half cycle starting from the open circuit voltage for each cell, sodium reacts with tin to form a series of Na−Sn alloys. The reactions involve forming the solid electrolyte interface (SEI), resulting in an irreversible capacity loss during the first cycle. The Coulombic efficiencies of the first cycle are 35%, 72% and 73% for $Sn_{0.9}Cu_{0.1}$, Sn nanoparticle and Sn microparticle electrodes, respectively. The low initial Coulombic efficiency of the $Sn_{0.9}Cu_{0.1}$ electrode may be attributed to the small primary crystallites seen by TEM, providing extra surface area for SEI formation. This is supported by the appearance of a shoulder above 0.5 V in the case of the $Sn_{0.9}Cu_{0.1}$ electrode (indicated by a red arrow in Figure 3a) in the initial sodium insertion process, a feature which is absent in the following cycles. A complementary EDS analysis was applied to characterize the SEI on the cycled electrodes made of $Sn_{0.9}Cu_{0.1}$ and Sn nanoparticles, respectively (see Figure S3 in the Supporting Information). Compared to the Sn nanoparticle electrode, the cycled $Sn_{0.9}Cu_{0.1}$ electrode showed stronger signals from sodium, fluorine, oxygen, and carbon, indicating that there was more SEI formed on the $Sn_{0.9}Cu_{0.1}$ electrode than on the Sn electrode. The likely composition of the FEC-derived SEI is sodium fluoride, sodium carbonate and polyene compounds based on this EDS analysis and a previous study reported by Nakai et al.[31] The low initial Coulombic efficiency of $Sn_{0.9}Cu_{0.1}$ could be a problem in those applications where the anode is paired with a cathode containing a limited amount of sodium. Although the first cycle efficiency of the $Sn_{0.9}Cu_{0.1}$ electrode is low, it increased to more than 95% from cycle 2 and eventually reached 99% at the end of 100 cycles (see Figure 2b). This is however, much lower than the ~99.99% Coulombic efficiency required for commercial cells. The voltage profiles of the $Sn_{0.9}Cu_{0.1}$ electrode are almost identical between cycle 20 and cycle 100, indicating that the addition of Cu in Sn improves the stability upon Na insertion/deinsertion. Sn has been shown to aggregate during lithiation,[21,22] and we believe that the same phenomena could happen during sodiation. It is possible that the better stability is due to the higher melting point of Cu_6Sn_5

dx.doi.org/10.1021/am4023994 | ACS Appl. Mater. Interfaces 2013, 5, 8273−8277

which suppresses electrochemical aggregation of the composite particles.

The electrochemical impedance spectroscopy (EIS) measurements of the electrodes made of $Sn_{0.9}Cu_{0.1}$ nanoparticles, Sn nanoparticles and Sn microparticles after 100 cycles at 0.2 *C* rate are shown in Nyquist plots (Figure 4). The measurements

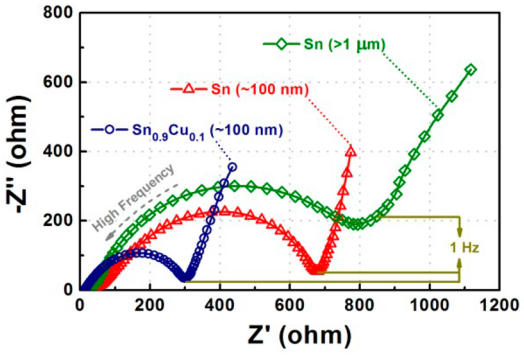

Figure 4. Electrochemical impedance spectroscopy of electrodes made of $Sn_{0.9}Cu_{0.1}$ nanoparticles, Sn nanoparticles, and Sn microparticles. All measured after 100 cycles at 0.2 *C* rate.

were carried out over a frequency range from 100 kHz to 0.05 Hz at 0.75 V with an AC perturbation voltage of 5 mV. Each plot consists of a semicircle in the high frequency region (>1 Hz) attributed to the charge transfer process, and a sloped line in the low-frequency region (<1 Hz) related to the mass transfer of Na^+. The charge-transfer resistance can be determined by measuring the diameter of the semicircle in the Nyquist plot. The electrode made of Sn microparticles has a large charge-transfer resistance, ~900 Ω, higher than that of the electrode made of Sn nanoparticles (~700 Ω). This suggests that after cycling, the transfer of electrons becomes more difficult in the electrode made of larger particles. This may be a result of the structural instability of Sn microparticles during the sodium insertion/deinsertion process. Compared to the electrodes made of Sn nanoparticles and Sn microparticles, the $Sn_{0.9}Cu_{0.1}$ nanoparticle electrode has a much smaller charge transfer resistance ~300 Ω, indicating that addition of copper in tin reduces the interfacial charge transfer resistance.

Electrodes made of $Sn_{0.9}Cu_{0.1}$ nanoparticles and Sn nanoparticles were also tested at higher current densities. The charge/discharge rate was increased stepwise from 0.2 *C* (169 mA g^{-1}) to 0.5 *C*, 1 *C* and 2 *C* (1694 mA g^{-1}), with each *C* rate for 20 cycles, as shown in Figure 5. The average reversible capacities of each electrode as a function of current density are shown in Figure S4 in the Supporting Information. The reversible capacities decrease with increasing current densities for all electrodes because the reactions are kinetically constrained at high rates. Nevertheless, the high-rate performance of the $Sn_{0.9}Cu_{0.1}$ electrode was much better than the Sn nanoparticle electrode. At current densities of 424, 847, 1694 mA g^{-1}, the $Sn_{0.9}Cu_{0.1}$ electrode retained capacities of 265, 182, 126 mA h g^{-1} while the Sn electrode retained only 222, 120, 50 mA h g^{-1}, respectively. Typical voltage profiles at various rates are shown in Figure 6. Compared to the Sn electrode, less potential polarization is observed between charge and discharge half-cycles for the $Sn_{0.9}Cu_{0.1}$ electrode at high rates, consistent with the lesser charge transfer resistance seen in the Nyquist plots of Figure 4. Furthermore, cycling at 0.2−2 *C* rates does not damage the $Sn_{0.9}Cu_{0.1}$ electrode, for which its capacity is

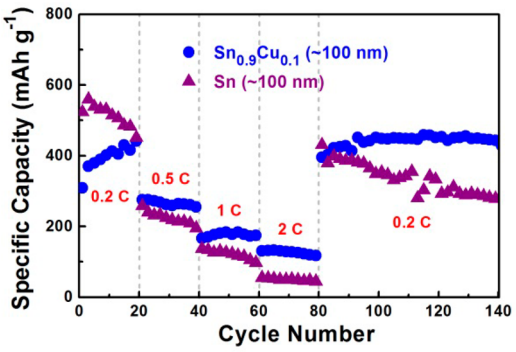

Figure 5. Reversible capacities of electrodes made of $Sn_{0.9}Cu_{0.1}$ nanoparticles and Sn nanoparticles cycled at various *C* rates from 0.2 to 2 *C*.

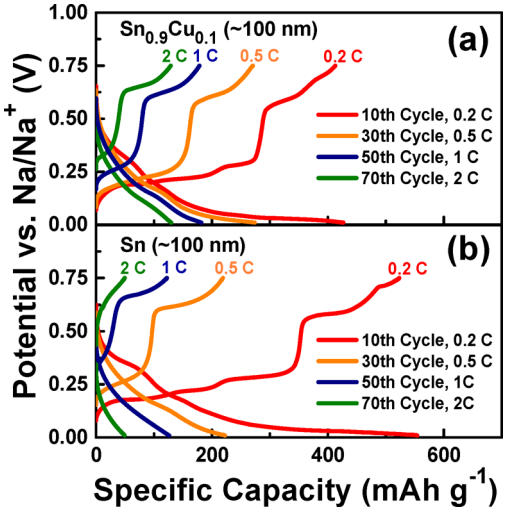

Figure 6. Voltage profiles of electrodes made of (a) $Sn_{0.9}Cu_{0.1}$ nanoparticles and (b) Sn nanoparticles cycled at various *C* rates from 0.2 to 2 *C*.

fully recovered upon returning to cycling at the 0.2 *C* rate, as shown in Figure 5.

CONCLUSION

In conclusion, $Sn_{0.9}Cu_{0.1}$ nanoparticles were prepared via a surfactant-assisted wet chemistry route carried out at room temperature, which were then investigated as an anode material for Na-ion batteries. Electrodes made with the $Sn_{0.9}Cu_{0.1}$ nanoparticles exhibit a stable capacity of greater than 420 mA h g^{-1} at 0.2 *C* rate, retaining 97% of their capacity after 100 cycles of sodium insertion/deinsertion. In contrast, electrodes made with Sn microparticles and Sn nanoparticles retained, respectively, only 13 and 49% of their capacities after 100 cycles at 0.2 *C* rate. The $Sn_{0.9}Cu_{0.1}$ electrode also showed better rate capability relative to a Sn nanoparticle electrode. The addition of copper in the tin was effective in reducing the interfacial charge transfer resistance enabling the high-rate capability of the anodes. Additionally, the cyclability of the anodes was improved, and we believe that the improvement was due to the suppression of aggregation among the nanoparticles.

dx.doi.org/10.1021/am4023994 | ACS Appl. Mater. Interfaces 2013, 5, 8273−8277

■ ASSOCIATED CONTENT

Supporting Information

Detailed experimental procedures, EDS elemental analysis results, additional SEM images, XRD patterns, high *C* rate test results. This material is available free of charge via the Internet at http://pubs.acs.org.

■ AUTHOR INFORMATION

Corresponding Author

*E-mail: mullins@che.utexas.edu.

Notes

The authors declare no competing financial interest.

■ ACKNOWLEDGMENTS

The Welch Foundation supported Y.-M.L. and A.H. (through Grant F-1131), J.B.G. (through Grant F-1066), and C.B.M. (through Grant F-1436). Y.-M.L. is also grateful for a Powers Graduate Fellowship from the University of Texas at Austin. P.R.A. acknowledges the Hertz Foundation for a graduate fellowship. The authors thank Solvay Special Chemicals for providing the FEC and Celgard for providing the separator material used in the coin cells.

■ REFERENCES

(1) Tarascon, J. M.; Armand, M. *Nature* **2001**, *414*, 359−367.
(2) Chalk, S. G.; Miller, J. E. *J. Power Sources* **2006**, *159*, 73−80.
(3) Kim, S. W.; Seo, D. H.; Ma, X. H.; Ceder, G.; Kang, K. *Adv. Energy Mater.* **2012**, *2*, 710−721.
(4) Dunn, B.; Kamath, H.; Tarascon, J. M. *Science* **2011**, *334*, 928−935.
(5) Teng, F. Z.; McDonough, W. F.; Rudnick, R. L.; Dalpe, C.; Tomascak, P. B.; Chappell, B. W.; Gao, S. *Geochim. Cosmochim. Acta* **2004**, *68*, 4167−4178.
(6) Seyfried, W. E.; Janecky, D. R.; Mottl, M. J. *Geochim. Cosmochim. Acta* **1984**, *48*, 557−569.
(7) Lu, X. C.; Xia, G. G.; Lemmon, J. P.; Yang, Z. G. *J. Power Sources* **2010**, *195*, 2431−2442.
(8) Sudworth, J. L. *J. Power Sources* **2001**, *100*, 149−163.
(9) Lu, Y. H.; Wang, L.; Cheng, J. G.; Goodenough, J. B. *Chem. Commun.* **2012**, *48*, 6544−6546.
(10) Wang, L.; Lu, Y. H.; Liu, J.; Xu, M. W.; Cheng, J. G.; Zhang, D. W.; Goodenough, J. B. *Angew. Chem., Int. Ed.* **2013**, *52*, 1964−1967.
(11) Stevens, D. A.; Dahn, J. R. *J. Electrochem. Soc.* **2001**, *148*, A803−A811.
(12) Qian, J. F.; Chen, Y.; Wu, L.; Cao, Y. L.; Ai, X. P.; Yang, H. X. *Chem. Commun.* **2012**, *48*, 7070−7072.
(13) Darwiche, A.; Marino, C.; Sougrati, M. T.; Fraisse, B.; Stievano, L.; Monconduit, L. *J. Am. Chem. Soc.* **2012**, *134*, 20805−20811.
(14) Chevrier, V. L.; Ceder, G. *J. Electrochem. Soc.* **2011**, *158*, A1011−A1014.
(15) Slater, M. D.; Kim, D.; Lee, E.; Johnson, C. S. *Adv. Funct. Mater.* **2013**, *23*, 947−958.
(16) Ellis, L. D.; Hatchard, T. D.; Obrovac, M. N. *J. Electrochem. Soc.* **2012**, *159*, A1801−A1805.
(17) Yamamoto, T.; Nohira, T.; Hagiwara, R.; Fukunaga, A.; Sakai, S.; Nitta, K.; Inazawa, S. *J. Power Sources* **2012**, *217*, 479−484.
(18) Ellis, L. D.; Ferguson, P. P.; Obrovac, M. N. *J. Electrochem. Soc.* **2013**, *160*, A869−A872.
(19) Lu, L.; Sui, M. L.; Lu, K. *Science* **2000**, *287*, 1463−1466.
(20) McFadden, S. X.; Mishra, R. S.; Valiev, R. Z.; Zhilyaev, A. P.; Mukherjee, A. K. *Nature* **1999**, *398*, 684−686.
(21) Kim, C.; Noh, M.; Choi, M.; Cho, J.; Park, B. *Chem. Mater.* **2005**, *17*, 3297−3301.
(22) Li, H.; Shi, L. H.; Lu, W.; Huang, X. J.; Chen, L. Q. *J. Electrochem. Soc.* **2001**, *148*, A915−A922.
(23) Zhang, W. J. *J. Power Sources* **2011**, *196*, 13−24.
(24) Xu, Y. H.; Zhu, Y. J.; Liu, Y. H.; Wang, C. S. *Adv. Energy Mater.* **2013**, *3*, 128−133.
(25) Xiao, L. F.; Cao, Y. L.; Xiao, J.; Wang, W.; Kovarik, L.; Nie, Z. M.; Liu, J. *Chem. Commun.* **2012**, *48*, 3321−3323.
(26) Kim, M. G.; Sim, S.; Cho, J. *Adv. Mater.* **2010**, *22*, 5154−5158.
(27) Chen, J.; Yang, L.; Fang, S.; Hirano, S.-i. *J. Power Sources* **2012**, *209*, 204−208.
(28) Wang, J.; Du, N.; Zhang, H.; Yu, J.; Yang, D. *J. Phys. Chem. C* **2011**, *115*, 23620−23624.
(29) Baggetto, L.; Jumas, J.-C.; Gorka, J.; Bridges, C. A.; Veith, G. M. *Phys. Chem. Chem. Phys.* **2013**, *15*, 10885−10894.
(30) Qian, J.; Wu, X.; Cao, Y.; Ai, X.; Yang, H. *Angew. Chem.* **2013**, *125*, 4731−4734.
(31) Nakai, H.; Kubota, T.; Kita, A.; Kawashima, A. *J. Electrochem. Soc.* **2011**, *158*, A798−A801.
(32) Lin, Y. M.; Klavetter, K. C.; Abel, P. R.; Davy, N. C.; Snider, J. L.; Heller, A.; Mullins, C. B. *Chem. Commun.* **2012**, *48*, 7268−7270.
(33) Komaba, S.; Ishikawa, T.; Yabuuchi, N.; Murata, W.; Ito, A.; Ohsawa, Y. *ACS Appl. Mater. Interfaces* **2011**, *3*, 4165−4168.
(34) Kravchyk, K.; Protesescu, L.; Bodnarchuk, M. I.; Krumeich, F.; Yarema, M.; Walter, M.; Guntlin, C.; Kovalenko, M. V. *J. Am. Chem. Soc.* **2013**, *135*, 4199−4202.
(35) Komaba, S.; Matsuura, Y.; Ishikawa, T.; Yabuuchi, N.; Murata, W.; Kuze, S. *Electrochem. Commun.* **2012**, *21*, 65−68.
(36) Klavetter, K. C.; Wood, S. M.; Lin, Y.-M.; Snider, J. L.; Davy, N. C.; Chockla, A. M.; Romanovicz, D. K.; Korgel, B. A.; Lee, J.-W.; Heller, A.; et al. *J. Power Sources* **2013**, *238*, 123−136.
(37) Ryou, M. H.; Kim, J.; Lee, I.; Kim, S.; Jeong, Y. K.; Hong, S.; Ryu, J. H.; Kim, T. S.; Park, J. K.; Lee, H.; et al. *Adv. Mater.* **2013**, *25*, 1571−1576.
(38) Song, S.-W.; Striebel, K. A.; Reade, R. P.; Roberts, G. A.; Cairns, E. J. *J. Electrochem. Soc.* **2003**, *150*, A121−A127.